Experimental investigations on B2O3-Al2O3-SiO2 glass-ceramics with different K2O/Na2O ratios for sealing to Kovar alloy

JIA, Han, BAI, Jilin, AO, Cong, LIN, Tiesong, DENG, Wei, LI, Hong and XIONG, Dehua

Experimental investigations on B_2O_3-Al_2O_3-SiO_2 glass-ceramics with different K_2O/Na_2O ratios for sealing to Kovar alloy

Han Jia[a], Jilin Bai,*[,a] Cong Ao[a], Tiesong Lin[b], Wei Deng[c], Hong Li[a] and Dehua Xiong*[,a,b]

a. State Key Laboratory of Silicate Materials for Architectures, Wuhan University of Technology, Wuhan 430070, P. R. China.

b. State Key Laboratory of Advanced Welding and Joining, Harbin Institute of Technology, Harbin 150001, P. R. China.

c. Materials and Engineering Research Institute, Sheffield Hallam University, Sheffield S1 1WB, UK.

* Corresponding author: baijilin520@whut.edu.cn (J. Bai), xiongdehua2010@gmail.com (D. Xiong).

Abstract:

This work studied the effects of the K_2O/Na_2O ratio on the viscosity of B_2O_3-Al_2O_3-SiO_2 parent glass and the microstructure, physical, and chemical properties of the resulting glass-ceramics after heat treatment. Additionally, the effect of sealing temperatures on the sealing strength of glass-ceramics-to-Kovar was studied. The results show that the viscosity of parent glass increases with the increase in the R ($R=n(K_2O)/[n(Na_2O)+n(K_2O)]$) value , and the viscous activation energy of BAS parent glass is about 262.65-293.85 KJ/mol. After heat treatment, the parent glass precipitates the main crystalline phase of $Al_{0.52}Zr_{0.48}O_{1.74}$ (PDF#53-0294) and ZrO_2 (PDF#37-1484). As the R value gradually increases, the thermal expansion coefficient of glass-ceramics initially decreases before increasing within the range of 44.74×10^{-7} to 52.29×10^{-7} $°C^{-1}$. The density follows a similar trend, fluctuating between 2.40 and 2.45 g/cm^3. Meanwhile, the resistivity of the glass-ceramics steadily increases from $1\times10^{12.07}$ to $1\times10^{14.82}$ Ω·cm. Moreover, the resistivity of GcN-3 (R=1/2) sample remains excellent at high temperatures, maintaining 3.94×10^9 Ω·cm at 600 ℃. Subsequently，the BAS glass-ceramics sample GcN-3 (R=1/2) was sealed with Kovar alloy at temperatures range from 930 to 970℃. With the increasing of sealing temperature, the sealing strength increased from 0.51 to 2.10 MPa. In the process of sealing, with the increase of temperature, the iron in the Kovar

alloy and the silicon in the glass-ceramics diffused to produce effective sealing and formed different sealing layers. The sealing area was observed to consist of four distinct regions: the matrix alloy, the alloy iron-deficiency area, the iron-rich glass-ceramics and the matrix glass-ceramics.

Keywords: B_2O_3-Al_2O_3-SiO_2; Glass-ceramics; sealing glass; Kovar alloy；Sealing Strength

1. Introduction

The advancement of microelectronics and structural components is contributing to the growth of diversity among electronic components[1-3]. The working environment of electronic components is becoming increasingly complex. As a result, there are higher requirements for sealing materials as well. Commonly used sealing materials can be broadly categorized into three groups: metal materials, organic materials, and inorganic non-metallic materials. Glass is a traditional inorganic non-metallic material highly valued for its adjustable softening point and sintering temperature, thermal expansion coefficient, exceptional electrical insulation properties, high chemical stability, and remarkable mechanical strength[4-6]. Due to these characteristics, glass is widely used as a sealing material in electronic components.

Previous reports have indicated that, in order to obtain strong sealing strength when glass is sealed with other materials, several considerations must be satisfied. Firstly, the thermal expansion coefficient of the sealing glass must match that of the substrate material[7-9]. Failure to achieve this match might result in significant internal stress during the cooling process, directly leading to sealing failure. Secondly, the sealing glass needs to demonstrate good chemical stability to withstand various extreme conditions during actual usage [9]. Finally, the sealing glass must have good flowability. The proper sealing temperature needs to be determined

according to its fluidity in order to achieve optimum sealing strength[9-11]. Glass-to-metal seals are classified as matched or unmatched seals according to the characteristics of the difference in thermal expansion coefficients the metals and glass substrates[12-15]. Matched sealing is a form in which the expansion curves of glass and metal are close enough, and the glass and metal substrates could be sealed directly[16]. With the matched sealing, less interior stress was generated during the sealing process, resulting in an excellent sealing performance[17]. Unmatched sealing is another form of sealing in which the expansion coefficients of the metal and glass are different. When the glass and metal substrates were sealed successful, there will be generated large stress in the interface between the glass and metal substrates[13]. There are various ways to resolve the unmatched sealing originated from the mismatched thermal expansion coefficients. For example, compression sealing is one of the means used in unmatched seals. The thermal expansion coefficient of the outer metal (e.g. FN25 alloy) is greater than that of the sealing glass, while the expansion coefficient of the lead wire (e.g. Kovar alloy 4J29) is comparable to that of the sealing glass[14]. The glass is subjected to compressive stresses from the external case during the sealing process, especially during the annealing temperature down to room temperature. As the sealing surface of glass and metal is subjected to compressive stress, the high compressive strength of glass is fully utilized to avoid cracks, and

the finally result is forming a high-strength and highly stable sealing joint[15]. In addition, sealing glass materials can be categorized into amorphous glass and glass-ceramics based on whether they have been crystallized during the sealing process. Amorphous glass, characterized by the absence of crystal formation during sealing process, exhibits a favorable flowability and wettability, which makes it easier to spread between the interfaces. However, it is difficult to adjust the coefficient of thermal expansion of glass, and its sealing strength is lower compared to sealing with glass-ceramics. In general, ceramic-based materials have outstanding strength, stability and dielectric properties[18]. The sealing glass-ceramics contain both glass and crystal phases in the sealing layer, offering several advantages in enhancing sealing strength and chemical stability. Nevertheless, the presence of crystal phases increase the glass melt viscosity, making the wetting reaction with the substrate become more challenging and resulting in a higher sealing temperature[11].

Many reports have discussed various kinds of sealing glass with high-resistance at high-temperature. Ghosh et al.[19] reported that the BaO-CaO-Al_2O_3-SiO_2 glass could be sealed with commercial ferritic stainless steel (Crofer22APU) at 850 ℃, the glass exhibits a high resistivity of 7.6×10^7 Ω·cm at 700 ℃. Liu et al.[20] investigated the Bi_2O_3-B_2O_3-BaO-ZnO glass-ceramics with a thermal expansion coefficient ranging from 60-82×10^{-7} $℃^{-1}$, and the electrical resistivity for this glass-ceramics reaches

4.11×10^{14} Ω·cm at room temperature. Additionally, Kundu et al.[21] reported that $BaO\text{-}La_2O_3\text{-}Al_2O_3\text{-}B_2O_3\text{-}SiO_2$ glass sealed with commercial ferritic stainless steel (Crofer22APU) at 650℃, achieving an electrical resistivity of around 1.59×10^{7} Ω·cm. Tian et al.[22] reported the $B_2O_3\text{-}Al_2O_3\text{-}SiO_2\text{-}RO$ (BAS) glass presents high electrical resistivity of 1.2×10^{12} and 1×10^{11} Ω·cm at room temperature and 300 ℃, respectively.

The Kovar alloy, widely applied in the fabrication of vacuum electronic devices, transistors, as well as sealing plugs and relay casings, possesses a moderate thermal expansion coefficient within the range of $50\pm5\times10^{-7}$ $℃^{-1}$. Consequently, the thermal expansion coefficient of $B_2O_3\text{-}Al_2O_3\text{-}SiO_2\text{-}RO$ (BAS) glass is well-matched for sealing with Kovar alloy[23]. Alkali metal oxides typically play key roles in decreasing characteristic temperatures and adjusting the thermal expansion coefficient in the glass.

In this work, in order to fulfill the requirements for sealing high-temperature microelectronic components while maintaining high resistance, glass-ceramics was chosen as a sealing material in detail, the BAS glass-ceramics were adopted to seal Kovar alloy substrates, and the content of alkali metal oxides (K_2O and Na_2O) was systematically adjusted to investigate their impact on the crystallization behavior, thermophysical, and electrical properties of BAS glass. Then the selected BAS glass-ceramics were used in sealing experiments to determine the optimal sealing temperature and sealing strength. Lastly, the sealing mechanism of BAS

glass-ceramics and Kovar alloy was further discussed.

2. Experimental

2.1 Preparation of BAS glass-ceramics

Firstly, we fine-tuned the molar ratio of K_2O/Na_2O while keeping the total mass of alkali metal oxides as constant to obtain an optimal glass composition. The samples were named from "N-1" to "N-5", and the specific glass compositions are presented in Table 1. The raw materials used without any purification, included SiO_2 (AR, 96.0%), Al_2O_3 (AR, 94.0%), $CaCO_3$ (AR, 99.0%), H_3BO_3 (AR, 99.5%), K_2CO_3 (AR, 99.0%), Na_2CO_3 (AR, 99.8%), ZrO_2 (AR, 99.0%), ZnO (AR, 99.0%), and MgO (AR, 98.5%), which are provided by Sinopharm Chemical Reagent Co. Ltd. Typically, 170 g of these raw materials were weighted and well-mixed, and then the glass compound was transferred into an alumina crucible, which was placed in an electric furnace and kept at 1600 ℃ for 3 hours for melting, clarifying, and homogenizing. The resulting glass melt was then poured onto a pre-heated steel plate to form a bulk glass sample. Subsequently, the glass sample was immediately transferred into an annealing furnace and kept at 620 ℃ for 2h to eliminate internal stresses. Finally, the glass sample was slowly cooled to room temperature and was cut into small pieces for further characterization. The annealed glass was placed into a resistance furnace and nucleated at 900 ℃ for 30 minutes and crystallized at 1300 ℃

for 30 minutes to obtain glass ceramics.

Table 1. the designed chemical composition of N-Group glass (wt%).

Sample No.	$SiO_2+B_2O_3+Al_2O_3$	ZnO	CaO	Na_2O	K_2O	ZrO_2	$R=n(K_2O)/[n(Na_2O)+n(K_2O)]$
N-1	80.000	5.000	5.000	5.000	0.00	5.000	0
N-2	80.000	5.000	5.000	2.841	2.15	5.000	1/3
N-3	80.000	5.000	5.000	1.984	3.01	5.000	1/2
N-4	80.000	5.000	5.000	1.238	3.76	5.000	2/3
N-5	80.000	5.000	5.000	0.000	5.00	5.000	1

2.2 Sealing experiments of BAS glass-ceramics to Kovar alloy

Fig. 1 illustrates the sealing process of BAS glass-ceramics to Kovar alloy. The as prepared glass samples were crushed and ground, and then passed through a 200-mesh sieve to obtain glass-ceramics powder. First, the sealing glass-ceramics powder was obtained by evenly mixing the ground glass-ceramics powder and terpineol. Then, 0.10 g of the mixture was weighed and pressed into a square mold (10×10 mm) to form a glass-ceramics powder tablet. This glass-ceramics pellet was then placed between two pieces of Kovar alloy substrates (30×12×1 mm) to fabricate a sandwich structure. Finally, the sample with the sandwich structure was subjected to heat treatment in a tubular furnace under an N_2 atmosphere to achieve a well-sealed joint between Kovar alloy and glass-ceramics component. It is worth noting that the use of Kovar alloy plates is to facilitate the testing of sealing strength.

Fig. 1. The sealing process of Glass-ceramics to Kovar alloy substrate

2.2 Analytical methods

Firstly, the parent glass was crushed and 50.00 g was weighted for viscosity measurement by using a high-temperature viscometer (RHEO1600, POSMA, China). The temperature was raised from room temperature to 1600 ℃ and held for 1 hour, followed by a controlled cooling to 1250 ℃ while the viscosity of glass melt was recorded. Differential scanning calorimetry (DSC) analysis was performed on the parent glass powder using a thermal analyzer (STA449F3, Netzsch, Germany) in an air atmosphere. The test temperature was ramped up to 1450 ℃ at a rate of 10 ℃/min to obtain DSC curves, enabling the determination of nucleation and crystallization temperatures of the parent glass. X-ray diffraction (D8 Advance, Bruker, Germany) was employed to test these samples, and the crystal phases within the samples were analyzed

using relevant software. Microstructural characterization of the samples was carried out by using Fourier-transform infrared spectrometry (Nicolet 6700, Thermofisher, USA) and laser confocal micro-Raman spectrometry (LABHRev-UV, Bruker, Germany). The glass-ceramics samples were cut into the size of 25×5×5 mm to measure the thermal expansion through a dilatometer (DIL402SE, Netzsch, Germany) from room temperature to 1000 ℃ at the heating rate of 5 ℃/min. The density of the glass-ceramics was calculated through Archimedean method using an electronic balance (AUY120, Shimadzu, Japan). Microstructural observations of the glass-ceramics were conducted using field emission scanning electron microscopy (FESEM, Sigma 300, Zeiss, Germany). Prior to FESEM testing, the glass-ceramics bulk samples were etched in 5 wt% HF solution for 60 seconds, followed by ultrasonic cleaning in deionized water and ethanol. Moreover，the glass-ceramics powder was etched in 5 wt% HF solution for 60 seconds and then collected through centrifugation. The resulting powder was analyzed for crystal structure and morphology using transmission electron microscopy (TEM, Tecnai G2F30, FEI, USA).

The glass-ceramics samples were cut into 20×20×1 mm, and the room temperature resistivity was measured using a bulk/surface resistivity test equipment (BEST-212, Beiguang, China), each sample were tested 9 times to obtain an average value. Furthermore, the temperature dependence of resistivity was evaluated using a physical property measurement system

(PPMS, Quantum, USA).The glass-ceramics samples were cut into the size of 10×10×1 mm and the temperature range was set from room temperature to 600 ℃ with a heating rate of 2 ℃/min. A piece of glass-ceramics block (10×10×2 mm) was immersed in deionized water, heated in a water bath at 90 ℃ for 10 h, and then the mass loss of the sample was calculated.

3. Results and discussion

3.1 Performance characterization of parent glass

Fig. 2 illustrated the high-temperature viscosity curves of the N-group glass with the test temperature decreasing from 1600 to 1250 ℃. Notably, the glass viscosity shows an increasing trend at the same temperature as the R value ($R=n(K_2O)/[n(Na_2O)+n(K_2O)]$) increased from 0 to 1, consistent with the typical behavior of molten glass. This phenomenon is attributed to the replacement of Na_2O by K_2O, both acting as network modifiers. Na^+ and K^+ ions reside within the interstitial voids of the structural network, providing free oxygen[24].

According to the prior research[25], the addition of alkali metal oxides, including of Li_2O, Na_2O, or K_2O in CaO-SiO_2-Al_2O_3 glass could reduce the viscosity of melts by introducing free oxygen to disrupt the network structure, which is following the order $Li_2O > Na_2O > K_2O$. As the R values increase, indicating a continuous substitution of Na_2O by K_2O while maintaining a constant content of total alkali metal oxides in the present

work. The proportion of K_2O in BAS glass gradually raised, leading to a decrease change trends in the quantity of free oxygen. This reduction in free oxygen corresponds to a diminished disruption of the glass network structure, resulting in a denser structure and an increased viscosity. Furthermore, the viscosity of glass melts is not only temperature-dependent but also associated with the activation energy of viscosity. Specifically, as the temperature increased, much more particles overcome the energy barriers, resulting in a rapid decreasement in glass melt viscosity. At high temperatures, the activation energy of viscosity can be approximated as a constant, which is following the Arrhenius equation (Eq.1)[26, 27].

$$\eta = A_0 \, \mathrm{Exp}\,(E_\eta / RT) \qquad \text{(Eq.1)}$$

where η is the viscosity of glass melt (Pa· s), E_η is the activation energy of viscosity, R is the molar gas constant (8.314J·mol^{-1}·K^{-1}), T is the absolute temperature, and A_0 is a temperature-independent coefficient.

By rearranging Eq.1 using the change of base formula, Eq. 2 could be obtained[26, 27]:

$$\log \eta = A + B(1000/T) \qquad \text{(Eq.2)}$$

where A and B represented temperature-independent coefficients. Table 2 presents the related parameters derived from Eq.2. With increasing of the R values from 0 to 1 (substitution of K_2O for Na_2O) the activation energy reaching a minimum value of 263.99 kJ/mol when R was 2/3 (sample N-3). Upon complete replacement of Na_2O in sample N-5, the activation

energy value increases to 293.85 kJ/mol, which is much higher than when alkali metal oxides are used in a mixed manner. This result may be due to the mixed alkali oxides effects in glass system. Wang et al.[27] have previously reported on the influence of mixed alkali oxides on the viscosity of MgO-Al_2O_3-SiO_2 glass, which demonstrated that mixed alkali metal oxides reduce viscosity and melting temperature more significantly compared to a single alkali metal. In this study, Initially, this substitution of K_2O for Na_2O in sample N-2 is primarily attributed to the network-breaking effect of free oxygen, leading to an increase in the activation energy for viscosity. With continued increasing K_2O addition, the mixed alkali effect may occur, resulting in a significant reduction in the activation energy for viscosity, and reaching a minimum value in sample N-3.

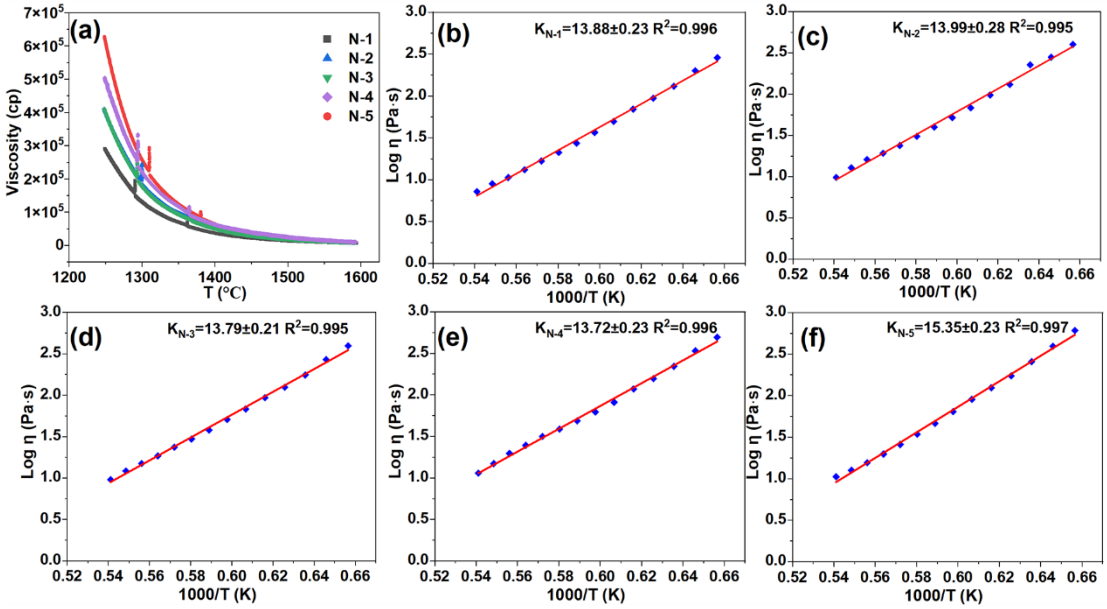

Fig. 2. High-temperature viscosity curves of the N-Group parent glass (a) and fitting curves for the viscosity activation energy of samples N-1 (b), N-2 (c), N-3 (d), N-4 (e), and N-5 (f).

Table 2. Fitting parameters and viscosity activation energy obtained from Equation 2.

Sample No.	A	B	E_η（KJ/mol）	R^2
N-1	-6.70±0.14	13.88±0.23	265.71	0.996
N-2	-6.59±0.13	13.99±0.28	267.82	0.995
N-3	-6.51±0.13	13.79±0.21	263.99	0.995
N-4	-6.38±0.16	13.72±0.23	262.65	0.996
N-5	-7.34±0.14	15.35±0.23	293.85	0.997

Fig. 3(a) presented the differential scanning calorimetry (DSC) curves for the N-groups parent glass. The glass transition temperature (T_g) was observed in the range of 633 to 651 ℃, and the T_g exhibits an overall upward trend with increasing the amount of K_2O. As K^+ gradually replaces Na^+ (increasing R values), resulting in the reduction in free oxygen. When the content of free oxygen was reduced, the net-breaking effect is weakened and the glass structure becomes more compact. The first weak exothermic peak temperature is located in the range of 958 to 895 ℃. The second exothermic peak is observed in the temperature range of 1202 to 1267 ℃, and its shape gradually become smoother with increasing the addition amount of K_2O. Moreover, the thermal stability of glass can be described by the temperature difference between glass transition

temperature and crystallization peak temperature (T_p), denoted as ΔT (Δ T=T_{p1}-T_g)[28]. The calculated ΔT from Fig. 3a indicated that all these N-group BAS parent glasses exhibit significant temperature differences, approximately around 244~324 ℃, which suggests these parent glasses have an excellent thermal stability. The specific values for thermal stability are presented in Table 3. Fig. 3b displayed the X-ray diffraction (XRD) spectrum for the N-groups BAS parent glass. It is evident from the absence of sharp/strong diffraction peaks, indicating that the prepared parent glass is amorphous state, showcasing a favorable glass-forming properties.

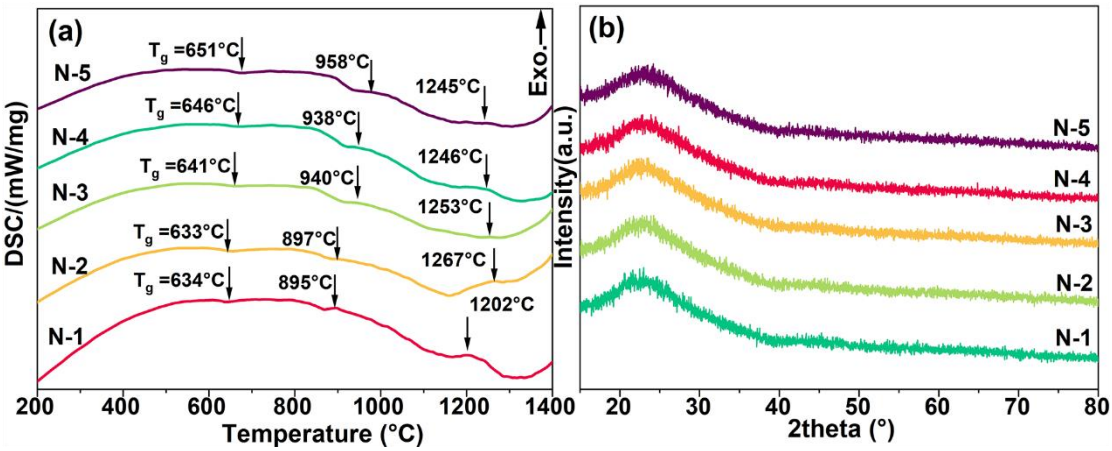

Fig.3. DSC curves (a) and XRD patterns (b) of N-group parent glass samples.

Table 3. Characteristic temperature values for N-groups BAS glass.

Sample No.	T_g (℃)	T_{p1} (℃)	T_{p2} (℃)	ΔT=T_{p1}- T_g (℃)
N-1	651	895	1245	244
N-2	646	897	1246	251
N-3	641	940	1253	299

N-4	633	938	1267	305
N-5	634	958	1202	324

Table 4. Heat treatment schedules for N-groups BAS glass.

nucleation		crystallization	
temperature/℃	time/min	temperature/℃	time/min
900	30	1300	30

3.2 Performance characterization of glass-ceramics

According to the results from Fig. 3, the heat treatment schedules for the preparation of BAS glass-ceramics were established, and the detailed information was outlined in Table 4. In fact, one-step crystallization heat treatment at 950 ℃ for 60 min has been tried in our previous experiments. The results showed streaky crystalline regions in the parent glass, and the glass and crystalline phases were spaced apart making the precipitation heterogeneous. In orders to achieve a better crystallization performance, we use a two-step method for heat treatment. For example, 900 ℃ for 30 min was used as nucleation treatment with the goal of forming many crystallizations nucleus. After that, the crystallization treatment was performed at 1300 ℃ for 30min, mainly to make the nucleus grow. Additionally, the nucleation of ZrO_2 is generally considered to be the precipitation of zirconium-oxygen-rich crystals from the parent phase, which induces the nucleation of the parent glass. Therefore, the above

mentioned discussion means the nucleation mechanism is heterogeneous for BAS glass-ceramics. For example, the nucleation and crystallization temperatures were set at 900 and 1300 °C, respectively, to prepare BAS glass-ceramics samples, and the glass-ceramics samples were recorded as "GcN-group". The XRD patterns of BAS glass-ceramics powder with different R values are shown in Fig. 4(a). The primary crystalline phases detected from the BAS glass are $Al_{0.52}Zr_{0.48}O_{1.74}$ (PDF#53-0294)[29, 30], ZrO_2 (PDF#37-1484)[29] and SiO_2 (PDF#85-0335). It is notable that SiO_2 is mainly present in GcN-1, while $Al_{0.52}Zr_{0.48}O_{1.74}$ and ZrO_2 are present in all glass-ceramics samples. These two crystalline phases have a tendency to enhance the intensity of the diffraction peaks with increasing R-value. The SEM images in Fig. 4(c-f) show the presence of a mixture of both spherical granular crystals and blocky columnar grains in these samples. Fig. 4(g) displays the EDS spectrum of spherical granular crystals in the GcGcN-3 sample, revealing that the crystals may correspond to $Al_{0.52}Zr_{0.48}O_{1.74}$, consistent with the XRD results in Fig. 4(a). Fig. 4(h) presents the EDS spectrum of blocky columnar grains in the GcGcN-3 sample. It is observed that both Zr and O elements are present, which could be assigned to the ZrO_2 crystal in glass-ceramics sample. Previous literature[31] has reported that ZrO_2 exists in a monoclinic crystal system at low temperatures, and the blocky columnar structures can form as the main crystalline phase in both monoclinic and triclinic crystal systems.

Therefore, the blocky columnar grains were identified as ZrO_2 in this work.

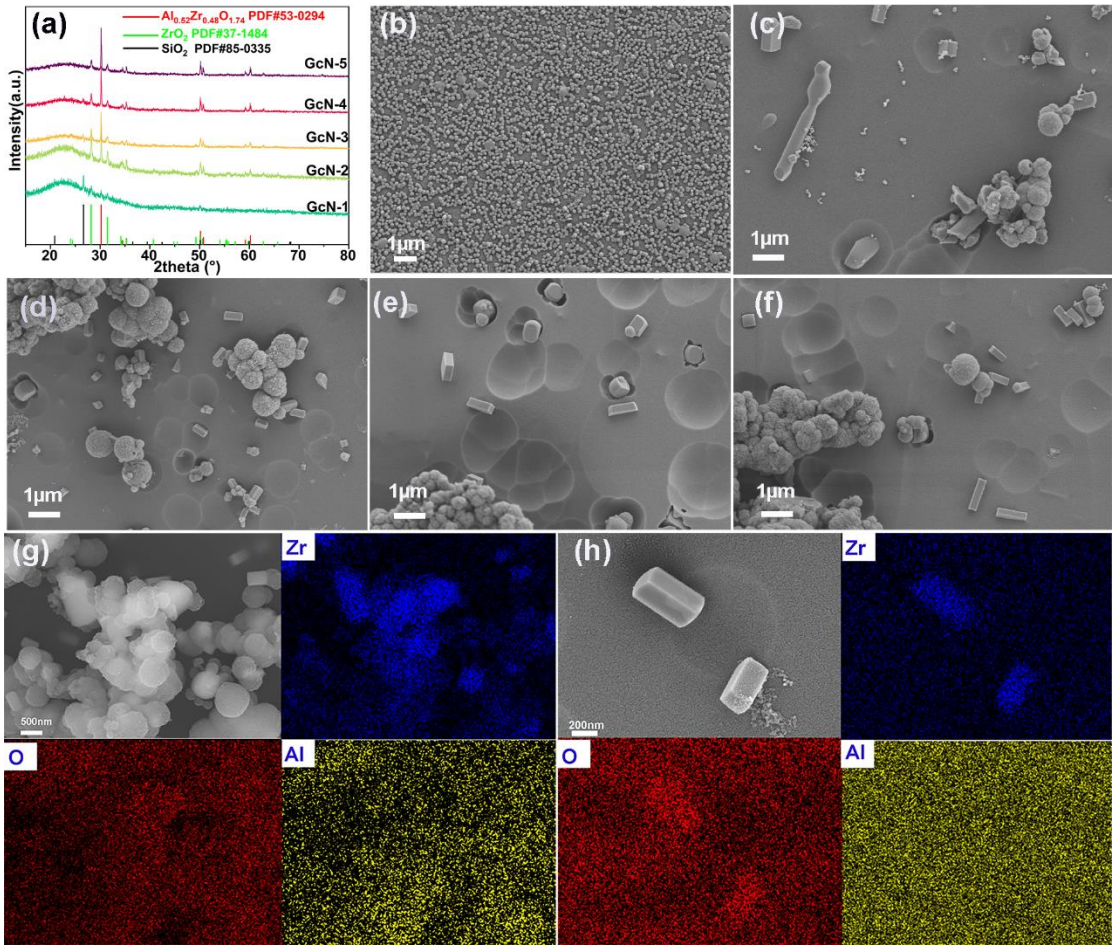

Fig. 4. XRD patterns of GcN-group BAS glass-ceramics (a), SEM images of GcN-1 (b), GcN-2 (c), GcN-3 (d), GcN-4 (e), GcN-5 (f), EDS spectra(g-f) of GcN-3 glass-ceramics.

Fig. 5 shows TEM images and EDS spectra of the GcN-3 glass-ceramics. The TEM image in Fig. 5(a) reveals spherical grains with a size of approximately 400 nm. By calibrating the electron diffraction pattern of the selected microcrystalline region in Fig. 5(b), the crystal lattice type was determined to be a tetragonal structure. The lattice fringe image in Fig. 5(c) was then used to determine the interplanar spacing to be 0.3060 nm. This interplanar spacing corresponds to the (101) crystal face of $Al_{0.52}Zr_{0.48}O_{1.74}$

(PDF#53-0294) crystals. The EDS spectrum mapping results in Fig. 5(d) confirm that the granular grains are $Al_{0.52}Zr_{0.48}O_{1.74}$ crystals with the tetragonal structure. Fig. 5(f) shows the selected-area electron diffraction pattern of blocky grains, confirming them to be monoclinic in nature through calibration. Fig. 5(e) displays the EDS spectrum mapping results of the blocky grains, combined with Fig. 5(f) of the selected-area electron diffraction pattern, confirming the monoclinic phase of ZrO_2 (PDF#37-1484). Our finding is consistent with other reports, Fritzsche reported the introduction of ZrO_2 into sodium borosilicate glass (NBS) and demonstrating its stabilizing effect on the initial glass phase separation and its catalytic effect on subsequent crystal growth. Zhang et al.[32] reported that during the sintering process, Mg^{2+} ions infiltrate into the M-ZrO_2 lattice to form C-$Zr_{0.8}Mg_{0.2}O_{1.8}$ solid solution. This low thermal expansion coefficient solid solution can prevent thermal stress cracking and damage, thereby improving the material's thermal stability. Based on this result, we can propose that Al^{3+} with ionic radii similar to those of Mg^{2+} may also enter the ZrO_2 lattice at high temperatures. Therefore, we believed that in our BAS glass-ceramics samples, with ZrO_2 as a nucleating agent and an appropriate amount of Al_2O_3, a small amount of Al^{3+} enters the lattice of tetragonal ZrO_2 phase at temperature over 1170 ℃, resulting in the formation of the tetragonal phase $Al_{0.52}Zr_{0.48}O_{1.74}$ solid solution at low temperatures. Meanwhile, the remaining tetragonal phase ZrO_2 undergoes

a phase transformation at temperatures below 400 °C, transforming into monoclinic zirconia.

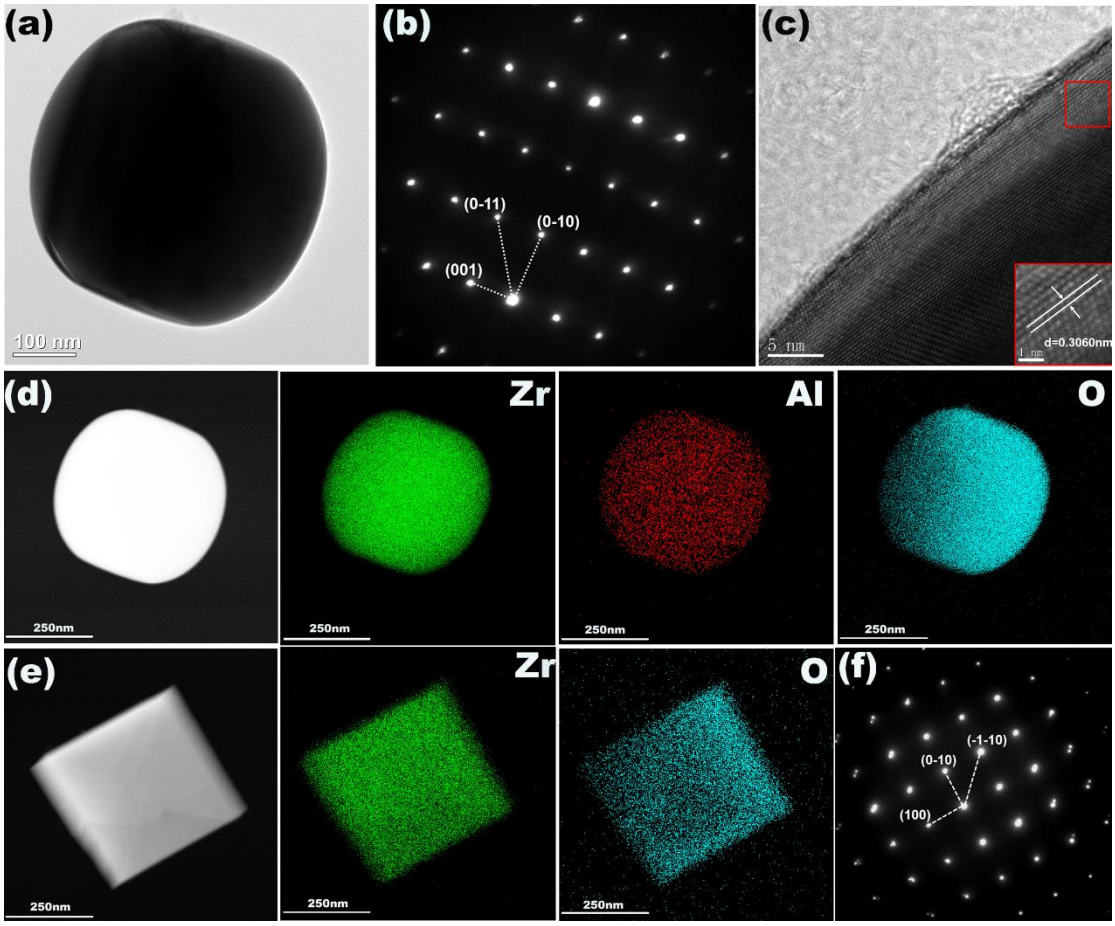

Fig. 5. TEM Image (a), granular crystallites SAED pattern (b), lattice fringe image (c), and EDS elemental mapping (d) of GcN-3. EDS elemental mapping of block-shaped crystallites (e) and SAED pattern (f) of selected area.

Both FTIR and Raman spectroscopy are commonly used to characterize the glass network structure. In Fig. 6(a) the FTIR spectrum of GcN-group samples depicts wavelength ranges from 400-2000 cm^{-1}. The absorption peaks positions in the FTIR spectrum were analyzed and listed in Table 6.

Infrared spectroscopy provides information about vibrations or rotations related to covalent bonds due to changes in molecular dipole moments. All these peak positions in the spectra of GcN-group samples didn't show significant changes, and no new peaks appeared with an increase in the R value. Several peaks are located near 450 cm^{-1}, 693-687 cm^{-1}, 796 cm^{-1}, 1070 cm^{-1}, 1094 cm^{-1}, and 1420 cm^{-1}. According to the literature, the absorption band at 450 cm^{-1} is mainly attributed to the bending vibration of Si-O-Si bonds, accompanied by some Si-O-Al vibration peaks overlapping[33-35]. The spectral bands around 693-687 cm^{-1} are attributed to the absorption peaks of bending vibration of five borate groups, which was composed of BO_4 and BO_3 units in a ratio of 1:4 in this glass-ceramics system[36-38]. The absorption peaks at 796 cm^{-1} and 1420 cm^{-1} are attributed to the asymmetric stretching vibrations of [AlO_4] and [BO_3] triangles, respectively[34, 35, 39]. Moreover, the vibration peak at 1070 cm^{-1} is assigned to the stretching vibration of B-O bonds in [BO_4] units[37, 39].In Fig. 6(b), the Raman spectrum of the GcN-groups samples with the wavelength ranges from 50-1000 cm^{-1} is presented. The positions of various peaks in the Raman spectra were analyzed and recorded in Table 7. It can be observed that the peak intensity increases with the increasing R value, possibly due to better crystallization in these glass-ceramics samples after heat treatment. The weakly peaks in sample GcN-1 may be attributed to factors such as fewer crystallites and smaller sizes in this sample. In

these Raman spectra, four distinct absorption bands are observed: (i) 95-180 cm^{-1}, (ii) 180-300 cm^{-1}, (iii) 300-550 cm^{-1}, and (iv) 550-650 cm^{-1}. In detail, the identified Raman bands in the low-frequency region at 95-180 cm^{-1} could be assigned to the vibrational modes of BO_3 and BO_4 units due to alkali-borates[37, 40]. The peak at 219 cm^{-1} indicates the presence of Zn-O tetrahedral bending vibrations of ZnO_4 units in the presented glass system[41]. The strongly polarized shoulder localized at about 264 cm^{-1} is ascribed to bending modes of ZnO_4 units[40]. Another bands ranging from 300 to 500 cm^{-1} are characteristic of mixed stretching and bending modes of Si-O-Si units[42]. The strong polarized peak located at around 470 cm^{-1} is attributed to the isolated vibrations of Si-O-Si and Si-O-B[42, 43]. The bands located at 550-650 cm^{-1} are usually assigned to the bending vibrations of bridging oxygen (BO) bonds of SiO_4[40]. However, the Raman peak intensity increases with the increasing of K_2O addition, maybe due to the different crystallization conditions of these BAS glass-ceramics. Therefore, the replacement of Na_2O with K_2O involves only a slight change in the amount of alkali metal oxide, specifically a variation in the content of free oxygen. This substitution does not lead to a significant change in glass network structure.

Fig. 6(c) presents the thermal expansion curve of the GcN-group glass-ceramics samples, with partial characteristic values summarized in Table 5. The linear thermal expansion coefficient (CTE) of glass-ceramics initially

decreased and then changes little with an increase in the R value, ranging from 44.74 to 52.30×10^{-7} $°C^{-1}$. The change trend of the glass softening point temperature was opposed to that of CTE, which increased from 630 °C to 742 °C. In this GcN-group BAS glass-ceramics, a minimum value of 44.74×10^{-7} $°C^{-1}$ is obtained for sample GcN-4 (R= 2/3).This result is consistent with a previous report by Li et al.[44], who replaced K_2O with Na_2O in B_2O_3-ZnO-Al_2O_3 glass systems. They found that as the number of non-bridging oxygen increases, the degree of connectivity and rigidity of the glass network decrease, leading to an increase in thermal expansion coefficient and a decrease in softening temperature of glass. Regarding the BAS glass in this work, the ionic radius of K^+ is larger than that of Na^+, and the smaller cation tightens the glass network. Therefore, doping a higher content of K^+ in the glass can reduce the thermal expansion coefficient. Moreover, when the R value increased, the overall number of free oxygens decreased due to the larger molar mass of K compared to Na. The reduction in free oxygen reduced the damage to the glass network structure, making the glass network structure denser and the thermal expansion coefficient decreased. Generally, the CTE of glass-ceramics is determined by both the glass phase and the residual crystal phase. The lower crystal content in GcN-1 has less effect on the CTE of glass-ceramics. The degree of crystallization of glass-ceramics tends to increase with the increased content of K_2O. Especially, the degree of crystallization is

significantly stronger in GcN-2 compared to that of GcN-1. As a result, a significant decrease in CTE was observed for GcN-2 glass-ceramics sample. However, the latter samples show less variation in the degree of crystallization, thus it makes the CTE mainly affected by the glass phase in glass-ceramics sample. At last, the presence of the mixed alkali oxides effect caused the thermal expansion coefficient to reach a minimum value when mixed alkali metals are used in sample GcN-4[45]. Additionally, the CTE of all these BAS glass-ceramics is around $47\pm5\times10^{-7}$ $°C^{-1}$, which matches well with that of the Kovar alloy substrate ($50\pm5\times10^{-7}$ $°C^{-1}$). Zanchetta et al.[46] reported that borosilicate glass for Kovar alloys are typically selected to have thermal expansion coefficients close to that of metal and as low as possible. Therefore, we propose that sample GcN-3 BAS glass-ceramics with a thermal expansion coefficient of 45.5×10^{-7} $°C^{-1}$ is more suitable for sealing Kovar alloys.

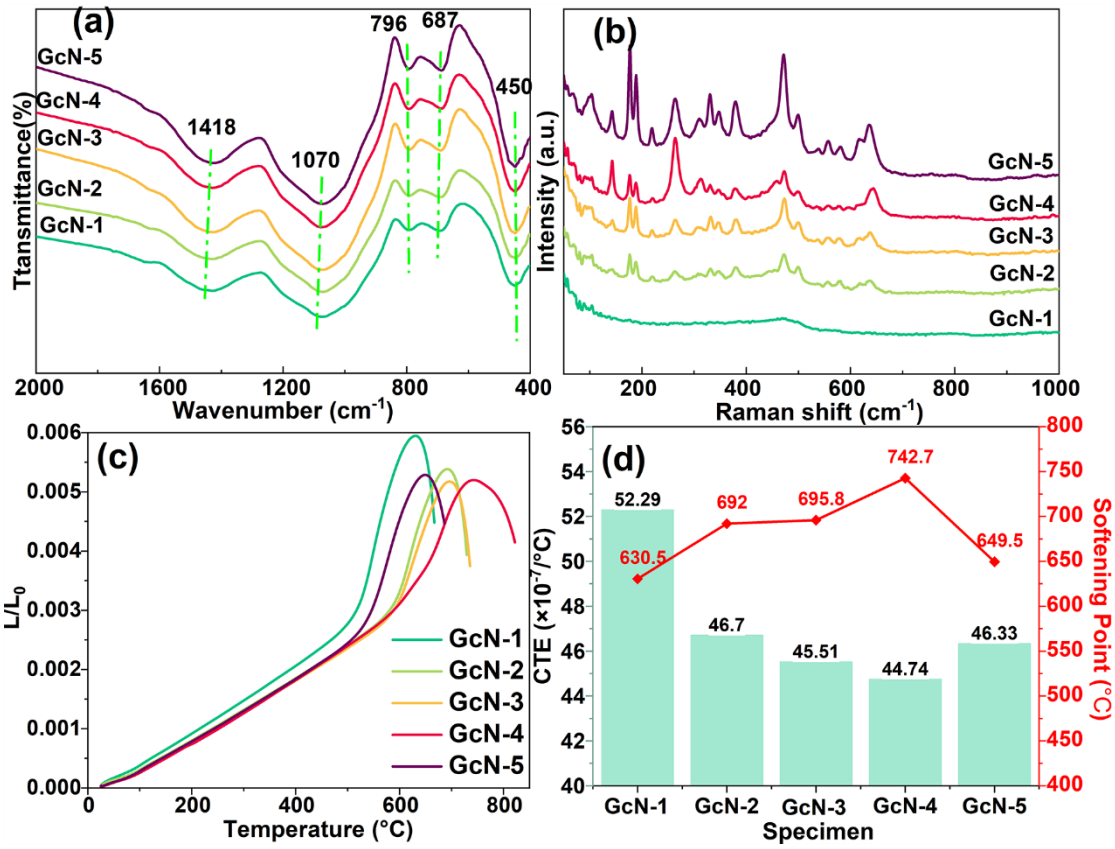

Fig. 6. FTIR spectrum (a), Raman spectrum (b), thermal expansion curve (c), and characteristic value variation curve (d) of GcN-groups samples.

Table 5. Characteristic values of GcN-group glass-ceramics.

Characteristic value	T_f（℃）	a×10^{-7}（$℃^{-1}$）
GcN-1	630	52.3
GcN-2	692	46.7
GcN-3	696	45.5
GcN-4	743	44.7
GcN-5	650	46.3

Table 6. Attribution of FTIR peaks in GcN-groups glass-ceramics.

Wavenumber	FTIR assignment

(cm^{-1})	
450	Si-O-Si bending vibration; asymmetric bending vibration of Si-O-Al[33-35].
693-687	Vibrations of pentaboranes groups, which are composed of BO_4 and BO_3 units in the ratio 1:4[37, 38].
796	The stretching vibration of Al-NBOs in [AlO_4][34, 35].
1070	The antisymmetric stretching vibration of Si-Ob-Si; B-O-B bending vibrations in [BO_4] units[37, 39].
1420	B-O stretching vibrations in BO_3units from boroxol rings[39].

Table 7. Attribution of Raman peaks in GcN-groups glass-ceramics.

Wavenumber (cm^{-1})	Raman assignments
104-190	The vibrational modes of BO_3 and BO_4 units due to alkaliborates[37].
219	Zn-O tetrahedral bending vibrations of ZnO_4 units[41].
264	Bending modes of ZnO_4 units[40].
300-500	Mixed stretching and bending modes of

	Si-O-Si units[42].
470	The stretching vibrations of Si-O-Si and B-O-Si[42, 43].
550-650	vibrations of the bridging oxygen (BO) bonds of SiO_4[40].

Moreover, density is an important parameter for evaluating the compactness of glass-ceramics. Fig. 7(a) shows the density test results of GcN-group BAS glass-ceramics samples, and the density of these samples around 2.40~2.45 g/cm^3. As the R value increased, the density of BAS glass-ceramics initially increases to a maximum value before slowly attenuating , indicating the presence of the mixed alkali oxides effect [47, 48]. Fig. 7(b) illustrates the water resistance of GcN-group BAS glass-ceramics samples after the stability test, the weight loss of these glass-ceramics around 0.30~0.38 wt% suggests an excellent water resistance. Generally, the erosion process of water on glass involves a displacement reaction between H^+ in water and network modifier ions in the glass structure[49]. The displacement reaction disrupts the glass structure, causing some components of the glass to dissolve into the solution, resulting in weight loss of the glass sample. As the R value increases, the high compactness of these BAS glass-ceramics increases with increasing R values, leading to the reduction of the amount of H^+ entering into the glass structure, which makes the dissolution of these samples more difficult.

Fig. 7(c) exhibits the electrical resistance values of the GcN-group BAS glass-ceramics samples at room temperature, and the volume resistivity of these samples around $10^{12.07}$~$10^{14.82}$ Ω·cm, which slowly increased with the increasing replacement of K^+ with Na^+.

In the case of glass, the primary carriers are typically alkali metal ions present in the glass matrix at room temperature[11]. As the larger K^+ ions radius encounters greater resistance during their directional movement within the BAS glass-ceramics, their conductivity decreases, exhibiting a higher resistance value. Additionally, when crystalline phases were precipitate in glass-ceramics samples, a greater number of precipitated crystals exert a more pronounced hindering effect on charge carriers, leading to an increasing trend in resistance. The temperature-dependent resistance curve of sample GcN-3 is shown in Fig 7(d). As the temperature increases from room temperature to 600 ℃, the resistance decreases from approximately 5.91×10^{13} Ω·cm to 3.95×10^{9} Ω·cm. This phenomenon is primarily attributed to the strengthening of molecular thermal motion and increased mobility of charge carriers, leading to enhanced conductivity and decreased resistance when the temperature was increased to 600 ℃. Moreover, the high stability of both ZrO_2 and $Al_{0.52}Zr_{0.48}O_{1.74}$ crystals at high temperature also contributes to the high resistance values of GcN-3 glass-ceramics sample, even at the high temperature of 600 ℃. It is essential to note that the electrical resistivity for the application is generally

required to be higher than 1×10^{10} Ω·cm at 150 ℃[50]. This results indicates the BAS glass-ceramics has excellent electrical insulation properties.

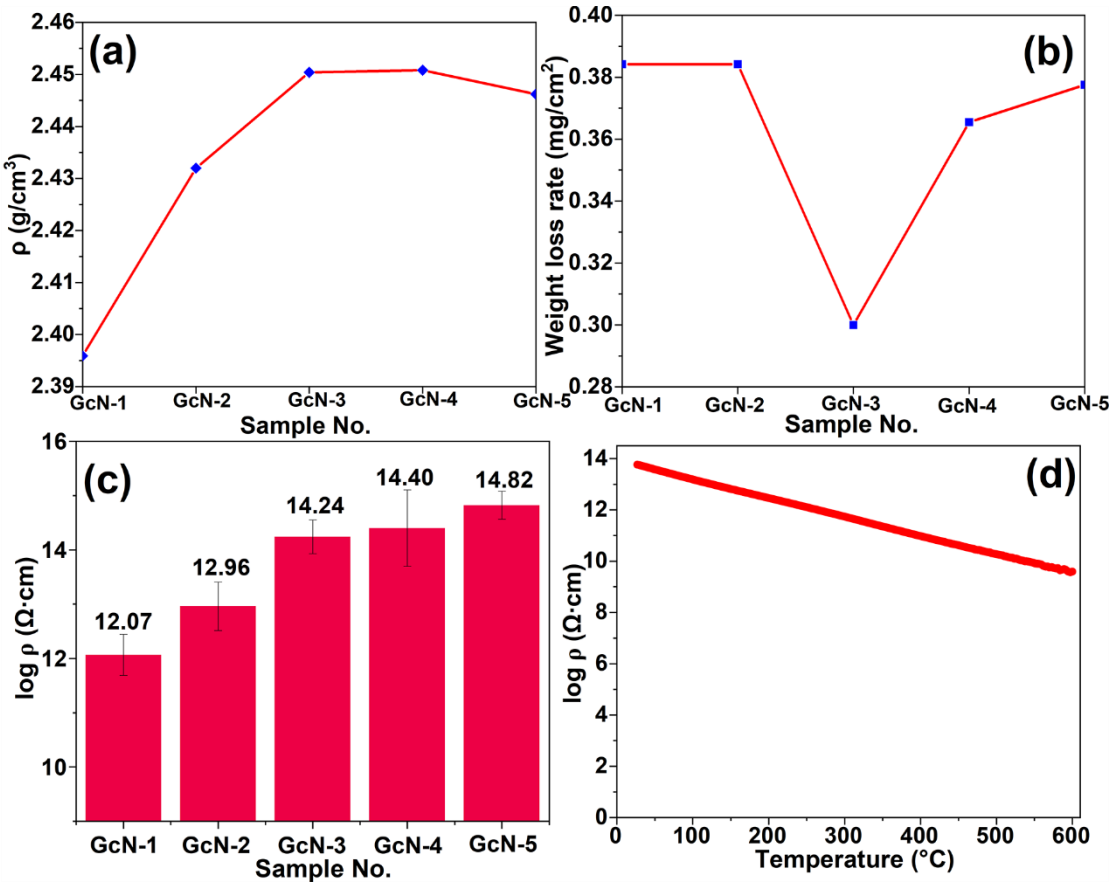

Fig.7. Density result (a), Water Resistance (b) and electrical resistivity of GcN-groups BAS glass-ceramics, and temperature-dependent electrical resistivity of sample GcN-3 (d).

Sealing glass/glass-ceramics should demonstrate favorable flowability and wetting properties when used in sealing applications with other materials. Assessing the appropriate operating temperature for sealing glass-ceramics involves examining their deformation behavior across various temperature ranges. In our experiment, we employed the button test method developed

by Owens-Illinois, which measures changes in column diameter to evaluate the flowability and deformation characteristics of the glass-ceramics under different temperatures.

Fig. 8(a) shows the deformation of BAS glass-ceramics samples at the temperature from 900 to 1025 ℃. The initial dimensions of all cylindrical samples in Fig. 8 are kept as the same, such as the height of 13.20 mm and the diameter (width) of 11.20 mm. Fig. 8(a) and 8(d) show the top-view and side-view appearance of these glass-ceramics samples as the temperature increases. Initially, the BAS glass-ceramics billets shrink and followed by the profiles becoming rounded at 1000 ℃. Moreover, the cylindrical samples transform into hemispheres and even flattening completely, as the temperature reached 1000 ℃. The temperature at which the corners begin to round and exhibit curved shapes is referred to as the corner rounding temperature (T_r), while the temperature at which the cylinder transforms into a hemisphere is known as the hemispherical point temperature (T_h)[11, 51]. These two characteristic temperatures corresponding to the viscosity values approximately to log η_{Tr}=6.3±0.1 and log η_{Th}=4.1±0.1, respectively[11, 51]. These temperatures usually correspond to the lower and upper temperature limits for the application of sealing materials. Both the lower and upper sealing temperatures for these BAS glass-ceramics are shown in Table 8, the minimum and maximum sealing temperature were around 900~950 ℃ and 950~1025 ℃,

respectively.

Fig. 8(b) and (c) illustrate the percentage of width expansion and height shrinkage of the cylindrical samples, respectively. This provides a clear view of the variations in height and width at different temperatures. With increasing temperature during thermal heat treatment, the height shrinkage increases from 0 to 70% approximately. And it gradually decreases with the addition of K_2O at the same temperature. In addition, the width expansion rate increases from approximately 0 to 140% with increasing heat treatment temperature. Similarly, the expansion rate gradually increases with the addition of K_2O at the same temperature.

Table 8. Optimal bonding temperature range for GcN-group Glass-ceramics.

Sample No.	minimum temperature (℃)	maximum temperature (℃)
GcN-1	900	950
GcN-2	900	975
GcN-3	925	975
GcN-4	925	975
GcN-5	950	1025

Comparing the deformation of cylindrical samples GcN-1 to GcN-5 at different temperatures suggests that the sealing temperature of glass-ceramics shows an increasing trend when R value increases. Meanwhile,

we observed that the spread width decreases as the R value increases at the same temperature, due to the deterioration in flowability of these glass-ceramics samples. The constant mass of alkali metal oxides results in a gradual reduction in free oxygen content as K^+ gradually replaces to Na^+. Free oxygen acts to break the glass network, resulting in a looser structure in the glass. As the content of free oxygen decreases, the network-breaking effect weakens, leading to a denser glass structure. Consequently, the glass viscosity gradually increases, resulting in smaller width expansion and exhibits different shape changes at the same temperature.

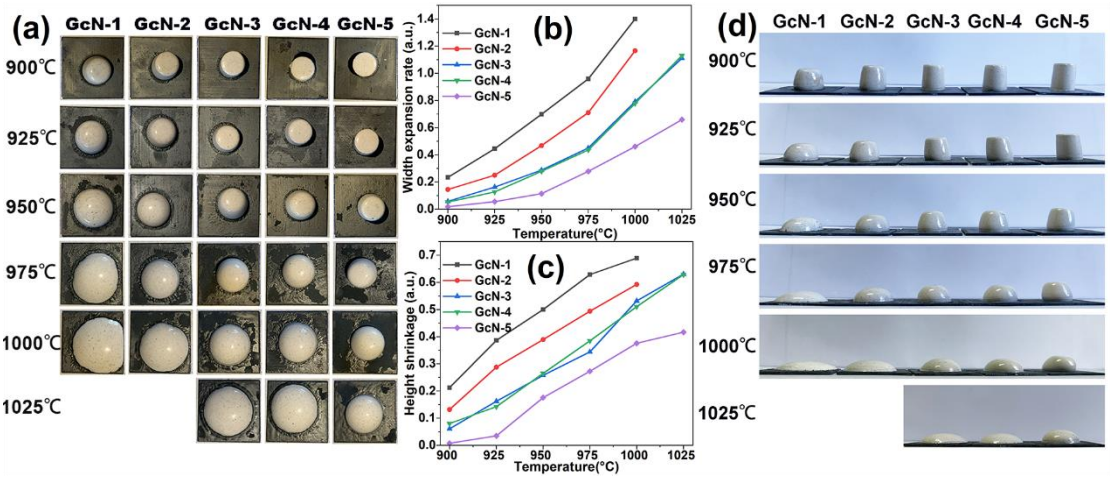

Fig. 8. Top view (a), side view (d), width expansion (b) and height shrinkage (c) of BAS glass-ceramics samples deformation at different temperatures.

Furthermore, we selected the GcN-3 glass-ceramics sample and applied a contact angle measurement instrument to analyze the contact situation between glass-ceramics and Kovar alloy substrate at high temperatures, such as the sealing temperature ranging from 900 to 975 ℃. In the glass-

metal matching sealing process, aside from the ordinary consideration of thermal expansion coefficients matching issue, it is also necessary to evaluate the wettability between glass and metal substrate [52, 53]. To improve the wettability between glass and metal, the surface of Kovar alloy usually pre-oxidized before the sealing experiment. This pre-treatment could generate an oxide layer on the surface of metal substrate, enhancing the wetting properties of sealing glass to metal substrate[10, 52, 53]. Therefore, we performed the pre-oxidized treatment of Kovar alloy at 850 ℃ for 10 minutes under a nitrogen atmosphere. Fig. 9(a) shows the contact angle photos of the GcN-3 sample on an unoxidized Kovar alloy, the sample was heated to 975 ℃ at a rate of 10 ℃/min. For comparison, the contact angle photos of the GcN-3 sample on a pre-oxidized Kovar alloy is shown in Fig. 9(b), which was heated to 975 ℃ and held for 60 minutes. Comparing with the contact angles of these two types of Kovar alloy, the pre-oxidized Kovar alloy exhibited better wettability with glass-ceramics at the same temperature. This result further confirms that the pre-oxidized treatment helps improve the wettability between sealing glass-ceramics and metal.

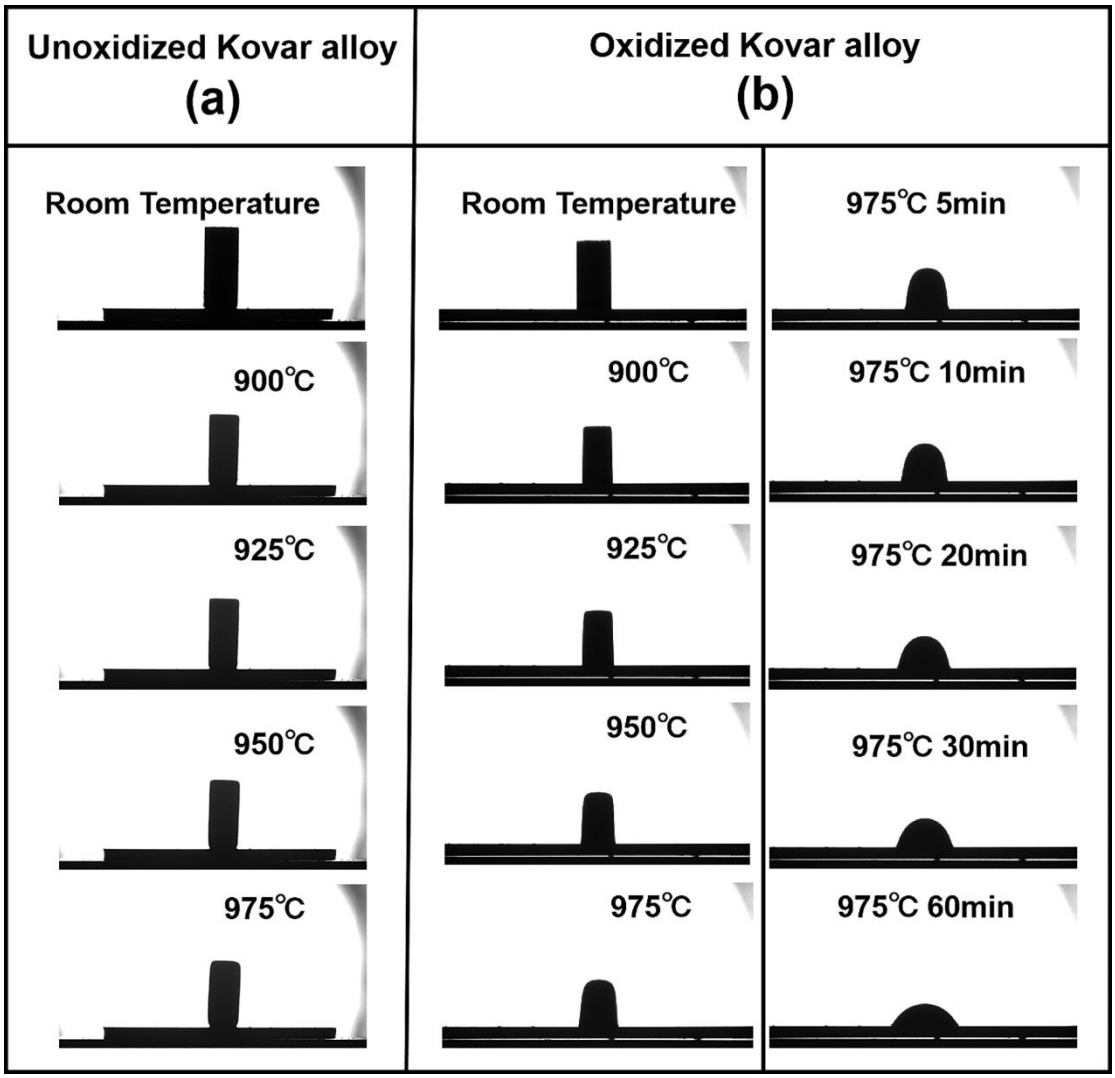

Fig. 9. High-temperature contact angle photos of GcN-3 sample heated to 975 ℃ on unoxidized carbide alloy at a rate of 10 ℃/min (a) and on oxidized carbide alloy at a rate of 10 ℃/min, held at 975 ℃ for 60 min (b).

3.3 Sealing between glass ceramics and Kovar alloy.

To further investigate the presence of the oxide layer originated from the pre-oxidized treatment, we conducted sealing experiments using both unoxidized and pre-oxidized Kovar alloy at 930 ℃. Fig. 10(a-c) shows the cross-sectional EDS results of the Kovar alloy and glass-ceramics sealed sample. By comparing the SEM images (Fig. 10(b) and (c)) of pre-oxidized

and unoxidized Kovar alloy, it was observed that the pre-oxidized Kovar alloy developed an oxide layer during the sealing process, serving as a transition layer for bonding between the Kovar alloy and glass-ceramics. A thin layer (with the thickness of 5~8 μm.) between the Kovar alloy and glass-ceramics were formed during the sealing process, consisting of iron, silicon, and oxygen. It was found that iron elements diffused to the sealing interface layer from the Kovar alloy substrate, whereas cobalt and nickel elements couldn't be detected. Meanwhile, both silicon and oxygen elements also spread from the glass-ceramics into the oxide layer. This result is in good agreement with other reports. Ardestani et al.[52] investigated the microstructure and mechanical properties of borosilicate glass sealing to Kovar alloy, they proposed that iron in the Kovar alloy is more likely to oxidize compared to nickel and cobalt. In other words, the oxide layer on the pre-oxidized Kovar alloy surface mainly consists of iron and oxygen, which is consistent with our findings in this study. Thus, the pre-oxidized Kovar alloy substrate was used in the following sealing experiment in our works. Fig. 10(d) shows the typical interface SEM image of GcN-3 glass-ceramics sealed to Kovar alloy at 970 ℃ for 30 minutes. The sealing interface can be divided into four regions: Region I and Region IV represent the sealing glass-ceramics and Kovar alloy, respectively. Region II shows the oxide interlayer originating from Kovar alloy dissolving and diffusing into the glass-ceramics, this region is enriched in

iron, silicon and oxygen elements and labeled as Fe-rich Zone. Region III is a region of Kovar alloy close to the oxide layer with relatively lower iron content, which is labeled as Fe-depleted Kovar. The above finding is consistent with a previous report. Dashtizad et al.[54] reported that pre-oxidation of Kovar alloy pulls out iron from the interior to form an oxide layer on the surface, leaving behind a region with less iron, resulting in voids due to iron loss. During the sealing experiments of BAS glass-ceramics to Kovar alloy in this work, silicon from the glass-ceramics can diffuse into the interior of Kovar alloy through these voids, consistent with the observations of this study.

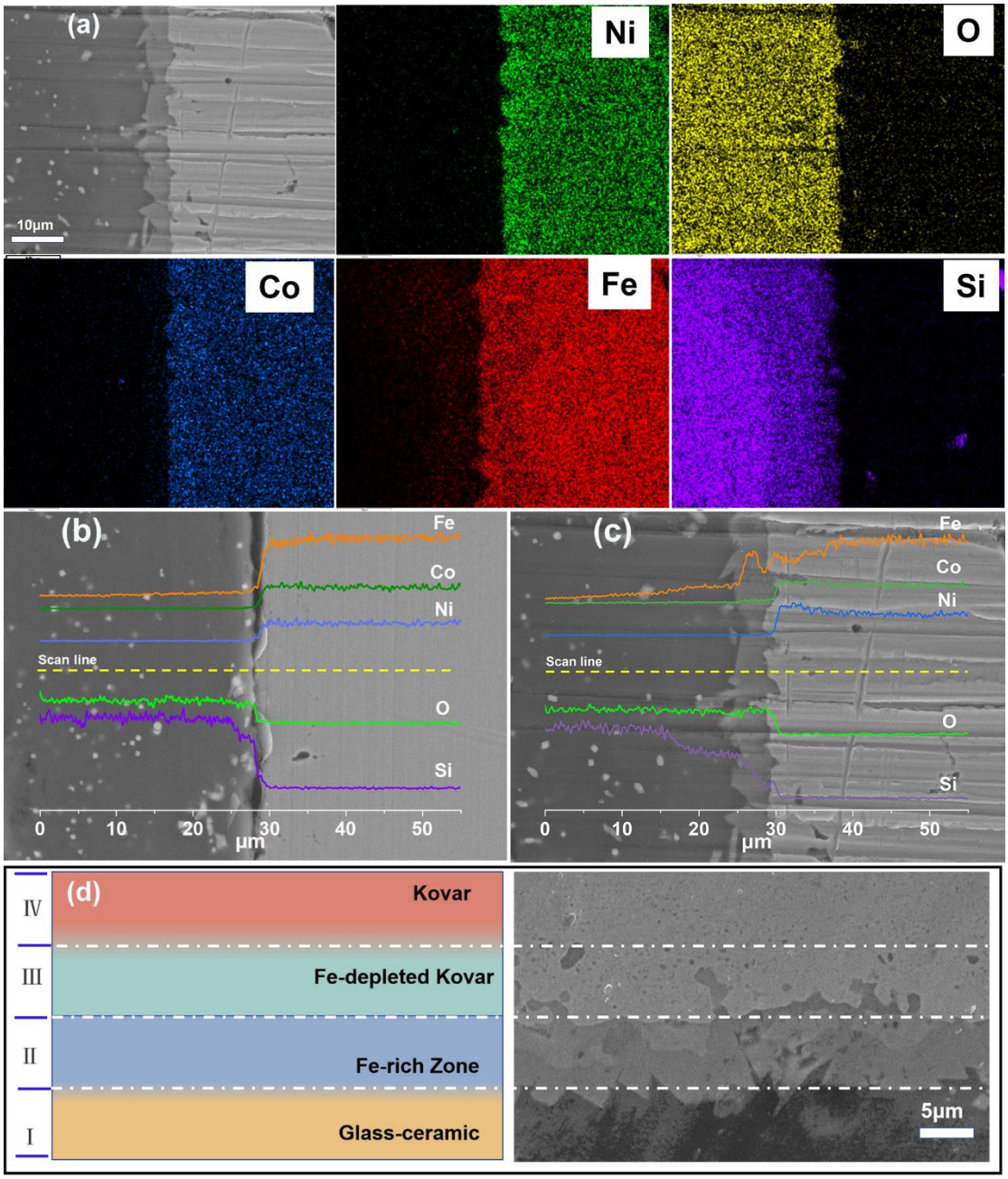

Fig. 10. EDS elemental mapping of the sealed interface between oxidized Kovar alloy and GcN-3 (a); line scan EDS spectra of (b) unoxidized and (c) oxidized Kovar alloy bonded with GcN-3 at 930 ℃; different regions (d) of the interface of bonded samples at 970 ℃.

To achieve the best sealing strength, we adjusted the sealing experiments at different temperatures for 30 minutes under an N_2 atmosphere, including

of 930 ℃, 940 ℃, 950 ℃, 960 ℃, and 970 ℃. Fig. 11(b) presents the shear strength of the GcN-3 sample at different temperatures. The sealing strength increases with the sealing temperature, and the maximum sealing strength of 2.107 MPa is achieved at 970 ℃. The cross-sections of the sealed samples were observed using SEM-EDS measurements. The cross-sectional line scan EDS results of these samples sealed at 930 ℃, 940 ℃, 950 ℃, 960 ℃, and 970 ℃ are shown in Fig. 11(c-g). The thickness of Fe-rich zone (Region II) increases with increasing the sealed temperature. For example, the thickness increased from 3 to 8 μm when the sealed temperature rose from 930 to 970 ℃. This Fe-rich region is formed by the Fe diffusion from the Kovar alloy surface into glass-ceramics, resulting in a relative enrichment of Fe elements. The shear strength of sealing samples is primarily influenced by the diffusion of elements (including of Fe, Si, etc.) contributing to mechanical bonding. BAS glass ceramic comes into direct contact with and penetrates the iron-deficient area of the Kovar alloy substrate in the sealing process. Simultaneously, the iron element in the oxide layer diffuses into the glass ceramic, which leading to the complete consumption of the oxide layer and the formation of a Fe-rich zone (Region II)[54, 55]. The extent of diffusion is influenced by experiment factors such as sealing temperature and time. Therefore, the diffusion process is more extensive at higher temperature, and thus the shear strength reaches the maximized value of 2.107 MPa at 970 ℃.

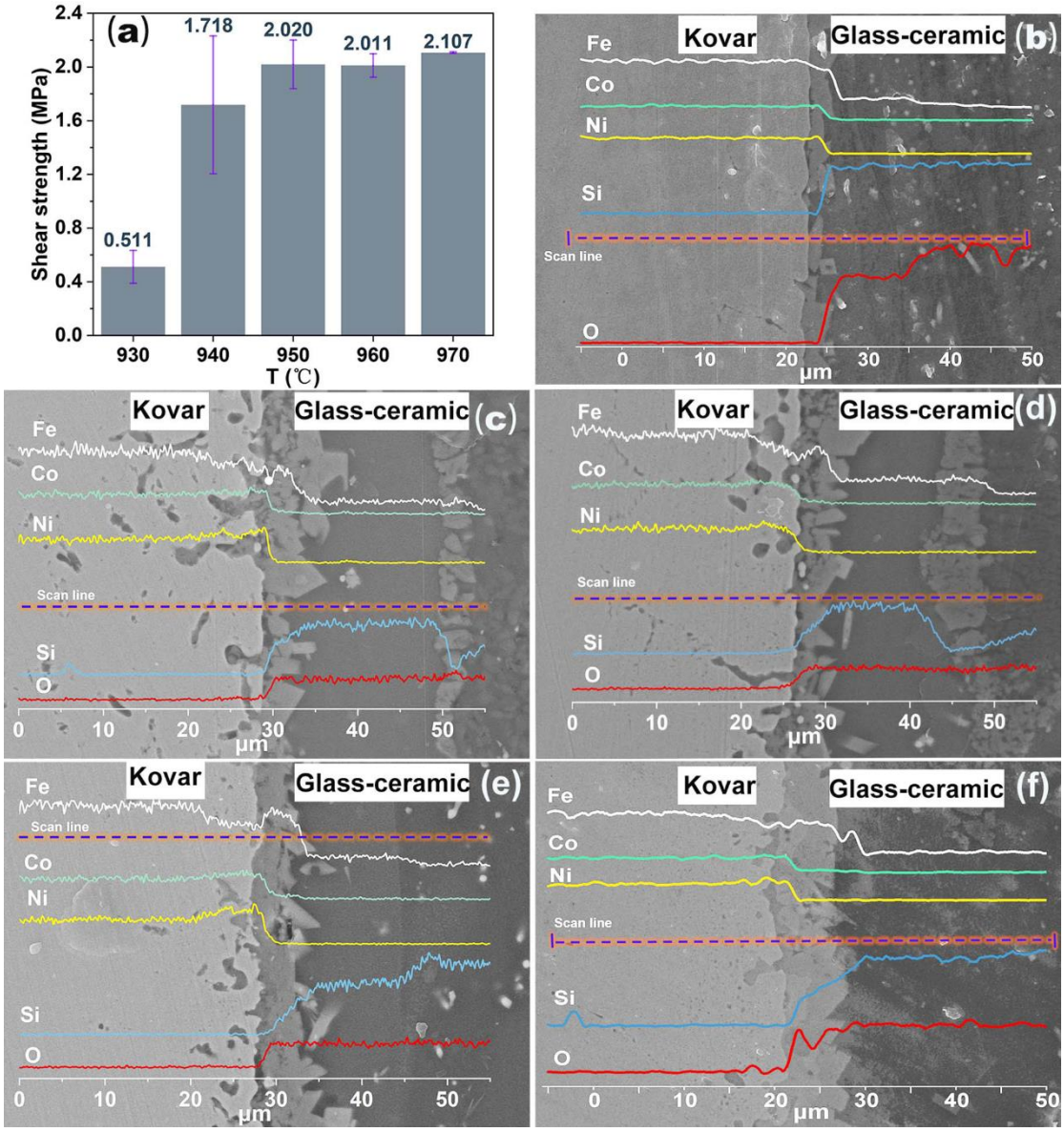

Fig. 11 Shear strength of GcN-3 sample sealed at different sealing temperatures (a), cross-sectional line scan EDS spectra of sealed samples at 930 ℃ (b), 940 ℃ (c), 950 ℃ (d), 960 ℃ (e), and 970 ℃ (f). Combined with the reports of Ardestani et al.[52, 54], we have proposed a possible sealing process of BAS glass-ceramics to Kovar alloy substrate in Fig. 12. Firstly, after the pre-oxidized treatment, an oxide layer with Fe rich region and a Fe-depleted region were formed on the surface of Kovar alloy substrate. When the sealing temperature raised, iron elements in the oxide

layer gradually diffuse into glass-ceramics, and the silicon elements in glass-ceramics also diffuse into oxide layer and Fe-depleted region. Lastly, the oxide layer gradually disappears and becomes a Fe-rich region due to the continuous diffusion of iron and silicon elements, and further diffusing into the glass-ceramics surface. Therefore, the sealing strength is mainly affected by the diffusion of these elements, especially for the mutual diffusion of silicon and iron during the dissolution of oxide layer, which is generally influenced by both the sealing temperature and sealing time. In detail, the oxide layer gradually dissolves onto glass-ceramics surface and undergoing a chemical reaction with SiO_2. The soften glass-ceramics comes into direct contact with the porous Fe-depleted region, finally silicon and iron elements diffusing internally and forming mechanical adhesion between glass-ceramics and Kovar alloy.

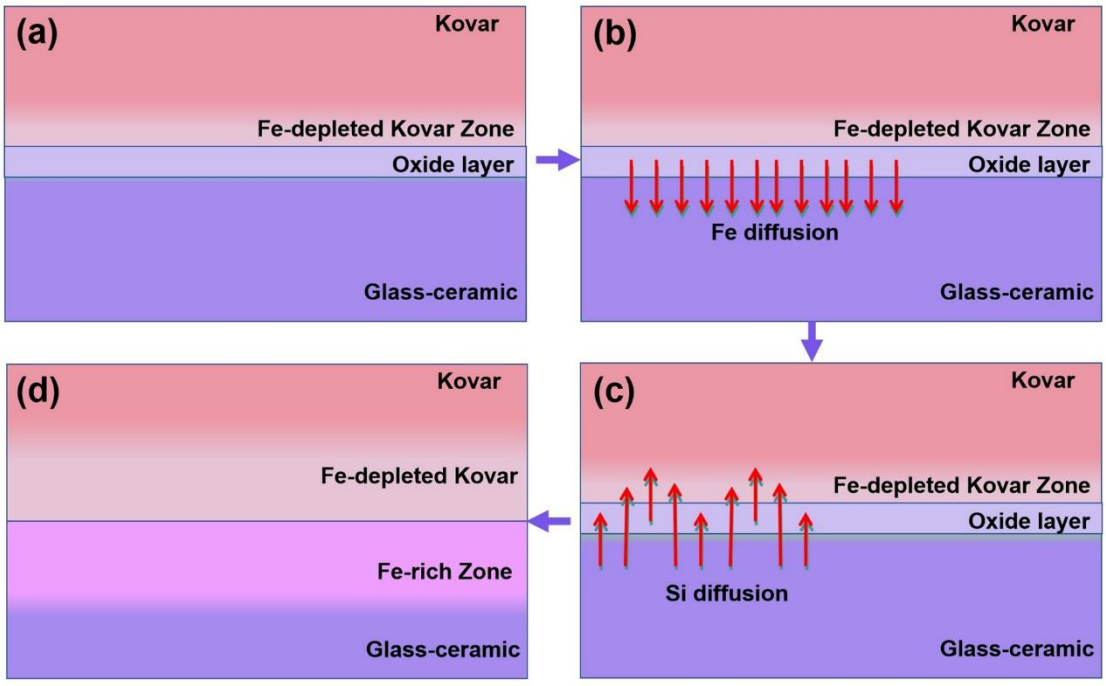

Fig. 12. Schematic representation of sealing process of glass-ceramics and

Kovar alloy.

4.Conclusion

In this study, we reported a B_2O_3-Al_2O_3-SiO_2 (BAS) glass-ceramics with an optimal ratio of K_2O/Na_2O, which was applied to sealing with Kovar alloy substrate. The effects of K_2O/Na_2O ratio on the viscosity of BAS parent glass, and the microstructure, physical, and chemical properties of BAS glass-ceramics were studied. The flowability of BAS glass-ceramics was observed through button experiments, and the sealing temperature range was determined. Finally, the effect of different sealing temperatures on the shear strength of glass-ceramics-to-Kovar sealing samples was studied. The conclusions are as follows:

(1) With the increase of R ($R=n(K_2O)/[n(Na_2O)+n(K_2O)]$) value, the amount of free oxygen is gradually reduced, the destruction of the glass network structure is reduced, and the glass structure becomes more compact, leading to an increase in viscosity. Moreover, the viscosity activation energy of the parent glass is about 262.65-293.85kJ/mol with the increase of R value.

(2) After heat treatment, the BAS parent glass precipitates $Al_{0.52}Zr_{0.48}O_{1.74}$ (PDF#53-0294) and ZrO_2 (PDF#37-1484). As the R value gradually increases, the thermal expansion coefficient of the glass-ceramics initially decreases before increasing within the range of 44.74×10^{-7} to $52.29\times10^{-}$

^{7} °C^{-1}, and the density follows a similar trend, fluctuating between 2.40 and 2.45 g/cm^{3}. Meanwhile, the resistivity of glass-ceramics steadily rises from $1\times10^{12.07}$ to $1\times10^{14.82}$ Ω·cm. Moreover, the resistivity of the GcN-3 (R=1/2) sample at high temperature is excellent, retaining 3.94×10^{9} Ω·cm at 600 ℃.

(3) The BAS glass-ceramics sample GcN-3 (R=1/2) was sealed with Kovar alloy at temperatures ranging from 930 to 970℃. With the increase in sealing temperature, the sealing strength increased from 0.51 to 2.10 MPa. During the sealing process, as the temperature rises, iron from the oxide layer gradually diffuses into glass-ceramic, while silicon from the glass-ceramic diffuses into the oxide layer and the iron-deficient area. Eventually, with the continuous diffusion of iron and silicon, the oxide layer diminishes, forming an iron-rich zone that further spreads to the glass-ceramic surface to create effective connections. It was observed that the sealing area could be divided into four different reigns: the matrix alloy, the alloy iron-deficiency area, the iron-rich glass-ceramics and the matrix glass-ceramics.

References

[1] J. Miao, H. Wang, P. Li, W. Shen, C. Xue, J. Xiong, Glass-SOI-based hybrid-bonded capacitive micromachined ultrasonic transducer with hermetic cavities for immersion applications, Journal of Microelectromechanical Systems, 25 (2016). 976-986. https://doi.org/10.1109/jmems.2016.2601312.

[2] Y. Leng, Y. Chen, Y. Yang, Y. Si, T. Xie, H. Wang, F. Meng, H. Ren, H. Lin, Tailoring the efficient laser-absorption-melting behavior of Bi_2O_3-B_2O_3-ZnO-Nd_2O_3 glass for the OLED encapsulation, Journal of the American Ceramic Society, 106 (2023). 2261-2270. https://doi.org/10.1111/jace.18911.

[3] H. Hamed, M. Eldiasty, S.-M. Seyedi-Sahebari, J.D. Abou-Ziki, Applications, materials, and fabrication of micro glass parts and devices: An overview, Materials Today, (2023). https://doi.org/10.1016/j.mattod.2023.03.005.

[4] H. Jia, L. Zhan, L. Han, X. Zhang, J. Xie, H. Li, D. Xiong, Effects of TiO_2 content and crystallization treatments on elastic modulus of alkali-free aluminosilicate glass, Journal of Solid State Chemistry, 325 (2023). 124177. https://doi.org/10.1016/j.jssc.2023.124177.

[5] Y. Yang, H. Ren, T. Xie, H. Peng, S. Jiang, Y. Zhang, F. He, D. He, H. Lin, The modification and strengthening dual functionality of rare-earth oxide in La_2O_3-BaO-SiO_2 glass for high temperature sealing application, Journal of Alloys and Compounds, 950 (2023). 169892. https://doi.org/10.1016/j.jallcom.2023.169892.

[6] L. Zhan, H. Jia, C. Jiang, T. Lin, H. Li, M. Wang, D. Xiong, Preparation and characterization of MgO-Al_2O_3-SiO_2 glass-ceramics with different MgO/Al_2O_3 ratio and La_2O_3 addition, Materials Today Communications, (2023). 107818. https://doi.org/10.1016/j.mtcomm.2023.107818.

[7] M. Telli, Soda Lime Silicate Glass Tube-Titanium Inset Joining by O_2/Propane Flame Work in Air, Acta Physica Polonica, A., 134 (2018). https://doi.org/10.12693/aphyspola.134.379.

[8] M.T. Staff, J.A. Fernie, P.M. Mallinson, M.J. Whiting, J.A. Yeomans, Fabrication of a glass-ceramic-to-metal seal between Ti-6Al-4V and a strontium boroaluminate glass, International Journal of Applied Ceramic Technology, 13 (2016). 956-965. https://doi.org/10.1111/ijac.12535.

[9] R.G. Frieser, A Review of Solder Glasses, Active and Passive Electronic Components, 2 (1975). 163-199. https://doi.org/10.1155/APEC.2.163.

[10] T.-S. Chern, H.-L. Tsai, Wetting and sealing of interface between 7056 Glass and Kovar alloy, Materials Chemistry and physics, 104 (2007). 472-478. https://doi.org/10.1016/j.matchemphys.2007.04.012.

[11] M. Wu, X.-b. He, Z.-s. Shen, X.-h. Qu, Preparation, crystallization, and wetting of ZnO-Al_2O_3-B_2O_3-SiO_2 glass-ceramics for sealing to Kovar, International Journal of Minerals, Metallurgy and Materials, 16 (2009). 586-591. https://doi.org/10.1016/S1674-4799(09)60101-1.

[12] Z. Fan, K. Hu, Z. Huang, Y. Zhang, H. Yan, Optimized sealing process and real-time monitoring of glass-to-metal seal structures, JoVE (Journal of Visualized Experiments), (2019). e60064. https://doi.org/10.3791/60064.

[13] R. Joshi, R. Chhibber, Development and interface characterization of unmatched glass-metal joint, Journal of Manufacturing Processes, 31 (2018). 787-800. https://doi.org/10.1016/j.jmapro.2017.12.027.

[14] D. Lei, Z. Wang, J. Li, J. Li, Z. Wang, Experimental study of glass to metal seals for parabolic trough receivers, Renewable Energy, 48 (2012). 85-91. https://doi.org/10.1016/j.renene.2012.04.033.

[15] R. Joshi, R. Chhibber, Effect of SiO_2/B_2O_3 ratio on the thermophysical and wetting properties of borosilicate glass sealant for glass-metal joint, Journal of Materials Processing Technology, 259 (2018). 186-194. https://doi.org/10.1016/j.jmatprotec.2018.04.028.

[16] R.H. Dalton, Solder glass sealing, Journal of the American Ceramic Society, 39 (1956). 109-112 https://doi.org/10.1111/j.1151-2916.1956.tb15633.x.

[17] K. Hu, H. Yan, Z. Fan, X. Diao, M. Liu, S. Li, Y. Zhang, In situ characterization of residual stress in glass-to-metal seal, Ceramics International, 45 (2019). 20983-20987. https://doi.org/10.1016/j.ceramint.2019.06.259.

[18] W. Luo, S. Yan, J. Zhou, Ceramic-based dielectric metamaterials, Interdisciplinary Materials, 1 (2022). 11-27. https://doi.org/10.1002/idm2.12012.

[19] S. Ghosh, A.D. Sharma, P. Kundu, S. Mahanty, R.N. Basu, Development and characterizations of BaO-CaO-Al_2O_3-SiO_2 glass-ceramic sealants for intermediate temperature solid oxide fuel cell application, Journal of Non-Crystalline Solids, 354 (2008). 4081-4088. https://doi.org/10.1016/j.jnoncrysol.2008.05.036.
[20] J. Liu, X. Xu, T. Zheng, Y. Guo, J. Lv, Effect of Bi_2O_3 content on the structure and properties of Bi_2O_3-B_2O_3-BaO-ZnO glass, Journal of Non-Crystalline Solids, 575 (2022). 121211. https://doi.org/10.1016/j.jnoncrysol.2021.121211.
[21] S. Ghosh, P. Kundu, A.D. Sharma, R.N. Basu, H.S. Maiti, Microstructure and property evaluation of barium aluminosilicate glass-ceramic sealant for anode-supported solid oxide fuel cell, Journal of the European Ceramic Society, 28 (2008). 69-76. https://doi.org/10.1016/j.jeurceramsoc.2007.05.008.
[22] Y.L. Tian, J. Zhang, S.B. Sun, J.Y. Fan, The Influence of Bi_2O_3 on SiO_2-Al_2O_3-B_2O_3-RO Glass Propertiesarts, Advanced Materials Research, 887 (2014). 86-89. https://doi.org/10.4028/www.scientific.net/AMR.887-888.86.
[23] D. Luo, Z. Shen, Wetting and spreading behavior of borosilicate glass on Kovar, Journal of Alloys and Compounds, 477 (2009). 407-413. https://doi.org/10.1016/j.jallcom.2008.10.028.
[24] Y. He, X. Shen, Y. Jiang, A. Lu, Effects of Li_2O replacing Na_2O on glass forming, structure and properties of Na_2O-MgO-Al_2O_3-SiO_2 glass and glass-ceramics, Materials Chemistry and Physics, 258 (2021). 123865 .https://doi.org/10.1016/j.matchemphys.2020.123865.
[25] Y. Hou, G.-H. Zhang, K.-C. Chou, D. Fan, Mixed alkali effect in viscosity of CaO-SiO_2-Al_2O_3-R_2O melts, Metallurgical and Materials Transactions B, 51 (2020). 985-1002. https://doi.org/10.1007/s12613-020-2187-9.
[26] C. Sun, S. Yang, L. Zhang, Y. Cao, Y. Qu, Y. Yue, J. Kang, High tensile strength glass fiber with different ratios of Na_2O and SiO_2 prepared by chemical strengthening method, Journal of Non-Crystalline Solids, 621 (2023). 122621. https://doi.org/10.1016/j.jnoncrysol.2023.122621.
[27] J. Wang, J.-s. Cheng, Z.-l. Deng, Effect of alkali metal Oxides on viscosity and crystallization of the MgO-Al_2O_3-SiO_2 glasses, Physica B: Condensed Matter, 415 (2013). 34-37. https://doi.org/10.1016/j.physb.2013.01.039.
[28] Y. Saddeek, E. Shaaban, F. Abdel-Rahim, K. Mahmoud, Thermal analysis and infrared study of Nb_2O_5-TeO_2 glasses, Philosophical Magazine, 88 (2008). 3059-3073. https://doi.org/10.1080/14786430802499012.
[29] Q. Gao, Y. Chen, N. Zhang, S. Chu, Z. Tao, R. Zhang, H. Li, Investigation on Preparation of $Al_{0.52}Zr_{0.48}O_{1.74}$ by Microwave Pyrolysis, in: IOP Conference Series: Materials Science and Engineering, IOP Publishing, 2019, pp. 012088. https://doi.org/10.1088/1757-899x/678/1/012088.
[30] H.-w. WANG, J.-x. WU, X.-y. WANG, W. Hong, J.-r. LIU, Formation of perovskite-type $LaNiO_3$ on La-Ni/Al_2O_3-ZrO_2 catalysts and their performance for CO methanation, Journal of Fuel Chemistry and Technology, 49 (2021). 186-197. https://doi.org/10.1016/s1872-5813(21)60012-9.
[31] J. Chevalier, L. Gremillard, A.V. Virkar, D.R. Clarke, The tetragonal-monoclinic transformation in zirconia: lessons learned and future trends, Journal of the american ceramic society, 92 (2009). 1901-1920. https://doi.org/10.1111/j.1551-2916.2009.03278.x.
[32] Y. Zhang, H. Gu, L. Fu, A. Huang, M. Zhang, Effect of pore structure and phase composition on thermal shock resistance of zirconia materials, Ceramics International, 49 (2023). 40120-40130. https://doi.org/10.1016/j.ceramint.2023.09.343.
[33] T. Sun, H. Xiao, W. Guo, X. Hong, Effect of Al_2O_3 content on BaO-Al_2O_3-B_2O_3-SiO_2 glass sealant for solid oxide fuel cell, Ceramics international, 36 (2010). 821-826 https://doi.org/10.1016/j.ceramint.2009.09.045.
[34] V. Kumar, S. Sharma, O. Pandey, K. Singh, Thermal and physical properties of 30SrO-40SiO_2-20B_2O_3-10A_2O_3 (A= La, Y, Al) glasses and their chemical reaction with bismuth vanadate for SOFC, Solid State Ionics, 181 (2010). 79-85. https://doi.org/10.1016/j.ssi.2009.12.005.
[35] E. Mansour, Semi-quantitative analysis for FTIR spectra of Al_2O_3-PbO-B_2O_3-SiO_2 glasses, Journal of non-crystalline solids, 358 (2012). 454-460. https://doi.org/10.1016/j.jnoncrysol.2011.10.037.
[36] G. Lakshminarayana, K.M. Kaky, S. Baki, A. Lira, P. Nayar, I. Kityk, M. Mahdi, Physical, structural, thermal, and optical spectroscopy studies of TeO_2-B_2O_3-MoO_3-ZnO-R_2O (R= Li, Na, and K)/MO (M= Mg, Ca, and Pb) glasses, Journal of Alloys and Compounds, 690 (2017). 799-

816. https://doi.org/10.1016/j.jallcom.2016.08.180.
[37] G. Lakshminarayana, S. Baki, A. Lira, I. Kityk, U. Caldiño, K.M. Kaky, M. Mahdi, Structural, thermal and optical investigations of Dy^{3+} doped B_2O_3-WO_3-ZnO-Li_2O-Na_2O glasses for warm white light emitting applications, Journal of Luminescence, 186 (2017). 283-300. https://doi.org/10.1016/j.jlumin.2017.02.049.
[38] A.E.C. Srinivasu, S. Rahman, K.S. Kumar, Infrared and Raman Spectroscopic Studies on mixed alkali tungsten based glasses, (2014). https://doi.org/10.1016/j.vibspec.2014.01.010.
[39] S. Rada, M. Culea, E. Culea, Structure of TeO_2· B_2O_3 glasses inferred from infrared spectroscopy and DFT calculations, Journal of Non-Crystalline Solids, 354 (2008). 5491-5495. https://doi.org/10.1016/j.jnoncrysol.2008.09.009.
[40] A.K. Yadav, P. Singh, A review of the structures of oxide glasses by Raman spectroscopy, RSC advances, 5 (2015). 67583-67609. https://doi.org/10.1039/c5ra13043c.
[41] S. Bale, S. Rahman, Spectroscopic and physical properties of Bi_2O_3-B_2O_3-ZnO-Li_2O glasses, International Scholarly Research Notices, 2012 (2012). https://doi.org/10.5402/2012/634571.
[42] B. Parkinson, D. Holland, M.E. Smith, C. Larson, J. Doerr, M. Affatigato, S.A. Feller, A. Howes, C. Scales, Quantitative measurement of Q^3 species in silicate and borosilicate glasses using Raman spectroscopy, Journal of Non-Crystalline Solids, 354 (2008). 1936-1942. https://doi.org/10.1016/j.jnoncrysol.2007.06.105.
[43] T. Rao, A.R. Kumar, K. Neeraja, N. Veeraiah, M.R. Reddy, Optical and structural investigation of Eu^{3+} ions in Nd^{3+} co-doped magnesium lead borosilicate glasses, Journal of alloys and compounds, 557 (2013). 209-217. https://doi.org/10.1016/j.jallcom.2012.12.162.
[44] A. Li, M. Wang, M. Li, Z. Liu, Y. Hu, X. Zhang, The effect of mixed alkali on structural changes and ionic migration characteristics in zinc borate glasses, Materials Chemistry and Physics, 217 (2018). 519-526. https://doi.org/10.1016/j.matchemphys.2018.07.013.
[45] Z.H. Xiao, A.X. Lu, F. Lu, Relationship between the Thermal Expansion Coefficient and the Composition for R_2O-MO-Al_2O_3-SiO_2 System Glass, Advanced Materials Research, 11 (2006). 65-68. https://doi.org/10.4028/www.scientific.net/AMR.11-12.65.
[46] A. Zanchetta, P. Lefort, E. Gabbay, Thermal expansion and adhesion of ceramic to metal sealings: case of porcelain-Kovar junctions, Journal of the European Ceramic Society, 15 (1995). 233-238. https://doi.org/10.1016/0955-2219(95)93944-X.
[47] X. Ma, Y. Xu, J. Cheng, S. Sun, Y. Chen, X. Wang, W. Chen, S. Chen, L. Hu, Influence of Mixed Na_2O/K_2O on Chemical Durability and Spectral Properties of P_2O_5-Al_2O_3-BaO-K_2O-Na_2O-Nd_2O_3 Phosphate Glasses, Materials, 15 (2022). 7439. https://doi.org/10.3390/ma15217439.
[48] J. Kjeldsen, M.M. Smedskjaer, J.C. Mauro, Y. Yue, On the origin of the mixed alkali effect on indentation in silicate glasses, Journal of Non-Crystalline Solids, 406 (2014). 22–26. https://doi.org/10.1016/j.jnoncrysol.2014.09.036.
[49] L. Deng, K. Miyatani, M. Suehara, S.I. Amma, J. Du, Ion-exchange mechanisms and interfacial reaction kinetics during aqueous corrosion of sodium silicate glasses, npj Materials Degradation, (2021). https://doi.org/10.1038/s41529-021-00159-4.
[50] D. Zhenbo, G. Shengxia, Z. Renjie, Lead-Free Sealing Glass Ceramics with High Thermal Expansion Coefficient, Low Softening Temperature and High Electrical Resistivity: An Overview, Journal of ceramics, 32 (2011). 256-268. https://doi.org/10.13957/j.cnki.tcxb.2011.02.029.
[51] J. Tong, M. Han, S.C. Singhal, Y. Gong, Influence of Al_2O_3 addition on the properties of Bi_2O_3-BaO-SiO_2-R_xO_y (R= K, Zn, etc.) glass sealant, Journal of non-crystalline solids, 358 (2012). 1038-1043. https://doi.org/10.1016/j.jnoncrysol.2012.01.044.
[52] S.S.K. Ardestani, V. Dashtizad, A. Kaflou, Experimental investigations on time, temperature and atmosphere influence on microstructure and mechanical properties of borosilicate glass to Kovar-alloy seals, Materials Characterization, 171 (2021). 110805. https://doi.org/10.1016/j.matchar.2020.110805.
[53] Z. Shen, Y. Zhang, Y. Chen, X. Song, T. Zhang, Effect of pre-oxidization condition on glass-to-metal sealing, Journal of Non-Crystalline Solids, 521 (2019). 119488. https://doi.org/10.1016/j.jnoncrysol.2019.119488.
[54] S.S.K. Ardestani, V. Dashtizad, A. Kaflou, Effects of temperature, time, atmosphere and sealing geometry on defects occurred in borosilicate glass-kovar alloy seal, Ceramics International, 47 (2021). 2008-2015. https://doi.org/10.1016/j.ceramint.2020.09.032.

[55] A. Zanchetta, P. Lortholary, P. Lefort, Ceramic to metal sealings: interfacial reactions mechanism in a porcelain-Kovar junction, Journal of alloys and compounds, 228 (1995). 86-95. https://doi.org/10.1016/0925-8388(95)01656-2.